

See discussions, stats, and author profiles for this publication at: <https://www.researchgate.net/publication/272834388>

# Sodium Bromide Induced Micelle to Vesicle Transitions of Newly Synthesized Anionic Surface Active Ionic Liquids Based on Dodecylbenzenesulfonate

ARTICLE *in* THE JOURNAL OF PHYSICAL CHEMISTRY B · FEBRUARY 2015

Impact Factor: 3.3 · DOI: 10.1021/jp512805e · Source: PubMed

---

CITATIONS

2

READS

41

## 5 AUTHORS, INCLUDING:



K. Srinivasa Rao

Sogang University

18 PUBLICATIONS 185 CITATIONS

[SEE PROFILE](#)



Praveen Singh Gehlot

Central Salt and Marine Chemicals Research I...

5 PUBLICATIONS 9 CITATIONS

[SEE PROFILE](#)



Hariom Gupta

21 PUBLICATIONS 77 CITATIONS

[SEE PROFILE](#)



Markus Drechsler

University of Bayreuth

196 PUBLICATIONS 6,743 CITATIONS

[SEE PROFILE](#)

# Sodium Bromide Induced Micelle to Vesicle Transitions of Newly Synthesized Anionic Surface Active Ionic Liquids Based on Dodecylbenzenesulfonate

K. Srinivasa Rao,<sup>†,‡</sup> Praveen Singh Gehlot,<sup>†,‡</sup> Hariom Gupta,<sup>‡</sup> Markus Drechsler,<sup>§</sup> and Arvind Kumar<sup>\*,†,‡</sup>

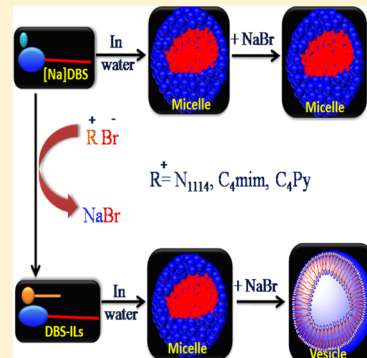
<sup>†</sup>Academy of Scientific and Innovative Research (AcSIR)-Central Salt and Marine Chemicals Research Institute, Council of Scientific and Industrial Research (CSIR), G. B. Marg, Bhavnagar 364002, Gujarat, India

<sup>‡</sup>CSIR-Central Salt and Marine Chemicals Research Institute, Council of Scientific and Industrial Research (CSIR), G. B. Marg, Bhavnagar-364002, Gujarat India

<sup>§</sup>Bayreuth Institute of Macromolecular Research (BIMF)—Soft Matter Electron Microscopy, Universität Bayreuth, Bld. NW II, D-95440 Bayreuth, Germany

## Supporting Information

**ABSTRACT:** Dodecylbenzenesulfonate-based anionic surface active ionic liquids (DBS-ILs) paired with onium cations, *n*-butyltrimethylammonium ( $[N_{1114}]$ ), 1-butyl-3-methylimidazolium ( $[C_4mim]$ ), and *N*-butylpyridinium ( $[C_4Py]$ ) have been synthesized. DBS-ILs were found to be highly surface active having critical micelle concentration (CMC) lower than that of their conventional analogue sodium dodecylbenzenesulfonate ( $[Na][DBS]$ ). The CMC values of DBS-ILs were determined from surface tension (ST) and isothermal titration calorimetry (ITC). DBS-ILs formed micelles predominantly in the aqueous medium, and unlike  $[Na][DBS]$ , the micelles of DBS-ILs could be transformed into vesicles with the addition of sodium bromide (NaBr). Micelle to vesicle transitions (MVTs) were evidenced from dynamic light scattering (DLS), turbidity, proton nuclear magnetic resonance ( $^1H$  NMR), and cryo-TEM techniques. Thermodynamics of aggregation was investigated from ITC which indicated that the aggregation process is primarily driven by the entropy factor. The formation of a vesicle upon addition of NaBr has been accounted to the increased electrostatic interactions between the less hydrated sulfonate headgroup and the more populated bigger sized counterions along with the favored cation- $\pi$  or  $\pi-\pi$  interactions between them as evidenced from 2D-NOESY NMR experiments. The stimuli-responsive morphological transitions in the self-assembly of the reported anionic surface active ionic liquids (SAILS) will be useful for encapsulation and delivery of active (bio)molecules in the targeted biomedical applications.



## 1. INTRODUCTION

Synthetic surfactant vesicles are widely studied colloidal structures due to their extensive applications such as mimics of biological membranes, microcompartments in the synthesis of inorganic nanomaterials, in encapsulation and controlled release of active molecules such as drugs in pharmaceutical applications, flavors and nutrients in foods, fragrances in cosmetics, and dyes in textiles.<sup>1–9</sup> Micelle to vesicle transition (MVT) is another extensively studied phenomenon in surfactant self-assembly because it offers encapsulation of active molecules in the micellar phase prior to vesicle formation enabling targeted encapsulation. MVT can be achieved by means of external stimuli such as pH, light, heat, cosurfactant, electrolyte, or  $CO_2$  in a single or mixture of surfactants.<sup>10–19</sup> The type of external stimuli that can drive MVT depends on the molecular structure of the surfactant.

Surface-active ionic liquids (SAILS, ionic surfactants with melting point below 100 °C) have been extensively studied in the past decade due to their unique nature that presents the properties of both surfactant and ionic liquid. Various classes of

SAILS such as cationic, anionic, catanionic, and zwitterionic have been developed and investigated for their self-assembly in a variety of solvent media.<sup>20–38</sup> SAILS have shown improved surface activity and emulsifying efficiency<sup>39</sup> compared to their conventional analogues along with some additional advantageous properties such as antimicrobial properties,<sup>40–42</sup> the ability to act as stabilizing and/or reducing agents in the synthesis of nanoparticles,<sup>35,43–45</sup> efficiency in the mitigation of algal blooms,<sup>27</sup> and improved solubility in hydrophobic IL medium.<sup>32</sup> Using SAILS, varieties of self-assembled structures have been constructed in both aqueous and ionic liquid media, including very advantageous vesicles and reverse vesicles.<sup>20–38,46–49</sup> Single-chain cationic and anionic SAILS have been shown to form vesicles spontaneously in combination with other oppositely charged surfactant/SAIL at appropriate mole fractions in aqueous media.<sup>50–54</sup> In some

Received: December 23, 2014

Revised: February 21, 2015

Published: February 27, 2015



of these mixed systems such as  $[C_8\text{mim}]Cl-[C_4\text{mim}]C_8\text{OSO}_3$ ,  $\text{CTAB}-[C_4\text{mim}]C_8\text{OSO}_3$ , and  $[C_{12}\text{mim}]Cl-[C_4\text{mim}]C_8\text{OSO}_3$  reversible MVTs have also been observed by varying the mole fraction of the mixture of SAIL–surfactant or two SAILS.<sup>45,53,54</sup> Cationic SAILS such as  $[C_8\text{mim}]C_8\text{OSO}_3$ ,  $[C_8\text{mim}]C_{12}\text{OSO}_3$ , and AOT-BHDC have also been shown to form vesicles in aqueous media without the aid of any external stimuli.<sup>33–35</sup> Unlike conventional cationic surfactants, long-chain imidazolium-based cationic SAILS ( $[C_n\text{mim}]Br$  ( $n = 10, 12, 14$ )) have shown spherical micelle to rod-like micelle to vesicle transitions with an increase in concentration in aqueous medium.<sup>55</sup> MVT is also observed in single-chain cationic SAIL  $[C_{12}\text{mim}]Br$  with the addition of 1-butyl-3-methylimidazolium 2-naphthalenesulfonate ( $[C_4\text{mim}]Nsa$ ) in an aqueous medium driven by the  $\pi-\pi$  interaction between the imidazolium headgroup of SAIL and the naphthalenesulfonate anion of additive IL.<sup>56</sup> Protic single-chain anionic SAIL diisopropylethylamine alkyl carboxylates  $[\text{DIPEA}][C_n\text{H}_{2n+1}\text{COO}]$  ( $n = 3–9$ ) are also shown to form vesicles spontaneously in aqueous media.<sup>57</sup> Very recently, we have reported vesicle formation by SAILS with double-chain anion dioctylsulfosuccinate (DSS) similar to its conventional analogue aerosol OT.<sup>32</sup> However, there are no reports on the vesicle formation and salt-induced MVT by aprotic single-chain anionic SAILS.

Herein, we have synthesized single-chain anionic surfactant-like ionic liquids based on the dodecylbenzenesulfonate anion (DBS-ILs) in combination of 1-butyltrimethylammonium, 1-butyl-3-methylimidazolium, and 1-butylpyridinium cations. The surface activity and self-assembly process of the synthesized DBS-ILs have been investigated in aqueous medium. Since the addition of electrolytes has been found to greatly influence the adsorption, CMC, shape, and size of the self-assembled structures of surfactant molecules through the immobilization of counterions in the stern layer,<sup>58,59</sup> we have also examined the salt effect on self-assembly of DBS-ILs. Among the alkali halides, NaBr has been shown to exhibit a unique effect on surface properties of anionic surfactants wherein the  $\text{Br}^-$  ions enhance the surfactant adsorption by causing the newly adsorbed surfactant molecules to adopt a vertical orientation at the air–water interface, whereas the adsorption enhancement ability of  $\text{Cl}^-$  and  $\text{I}^-$  is comparatively very less.<sup>58</sup> Therefore, NaBr is chosen to influence the surface properties of the DBS-ILs and induce MVT therein. Surface tension (ST), isothermal titration calorimetry (ITC), dynamic light scattering (DLS), turbidity, NMR, and cryo-TEM techniques have been employed to characterize the self-assembly process. The mechanistic insights of NaBr-induced MVT have been discussed in detail.

## 2. EXPERIMENTAL SECTION

**2.1. Materials.** Sodium dodecylbenzenesulfonate (>98% purity) and pyridine (>98% purity) were purchased from TCI Chemical (India) Pvt. Ltd. 1-Bromo butane of >98% purity was purchased from SRL, India. 1-Methyl imidazole was purchased from Spectrochem, India. Trimethylamine (30% aqueous solution), ethyl acetate, *n*-hexane, dichloromethane, diethyl ether, and toluene of AR grade were procured from SD-fine chem. Ltd., India. All the chemicals were of AR grade and were used as received. Millipore grade water with specific conductivity  $3 \mu\text{S}\cdot\text{cm}^{-1}$  and surface tension  $71 \text{ mN}\cdot\text{m}^{-1}$  was used for the study.

**2.2. Synthesis of Surface-Active Ionic Liquids.** (i). *Synthesis of n-Butyltrimethylammonium Bromide.* A 1:1.2 molar

ratio of trimethylamine (30% aqueous solution) and *n*-butyl bromide was dissolved in water in a round-bottom flask and refluxed in solution for 5 h; the progress of the reaction was checked by TLC. After completion of the reaction, water was removed at reduced pressures. The obtained reaction mixture was washed with ethyl acetate to remove the excess 1-bromobutane. Color impurities were removed by treatment with activated charcoal in methanol followed by the removal of solvent. The obtained brown waxy solid was characterized with LC–MS and  $^1\text{H}$  NMR techniques and dried for several hours using a rotary evaporator to remove moisture present prior to further use.

(ii). *Synthesis of N-Butylpyridinium Bromide.* A 1:1.2 molar ratio of pyridine and 1-bromobutane was dissolved in toluene and refluxed for 5 h, and the reaction was monitored by TLC and visual observation. After completion of the reaction the product present in the bottom layer was collected by decanting the solvent present in the upper layer. The obtained reaction mixture was washed with ethyl acetate to remove the excess 1-bromobutane present, and color impurities were removed by treatment with activated charcoal in methanol, followed by the removal of solvent. The obtained yellow oily liquid was characterized with LC–MS and  $^1\text{H}$  NMR techniques and dried for several hours using a rotary evaporator to remove moisture present prior to further use.

(iii). *Synthesis of 1-Butyl-3-methylimidazolium Bromide.* A 1:1.2 molar ratio of 1-methyl imidazole and 1-bromobutane was dissolved in toluene and kept under reflux conditions for 5 h. The reaction was monitored with TLC and visual observation. After completion of the reaction, the product at the bottom layer was collected by decanting the upper layer of solvent, and the residual solvent was removed under reduced pressures. Thus, the obtained product was washed with ethyl acetate 3 times to remove excess 1-bromobutane and dried for several hours using a rotary evaporator to remove the solvent and moisture present. The obtained pale-yellow viscous liquid was characterized using  $^1\text{H}$  NMR and LC–MS techniques.

(iv). *Synthesis of DBS-Based IL Surfactants (DBS-ILs).* Equimolar mixtures of  $[C_4\text{mim}]Br$  (or)  $[C_4\text{Py}]Br$  (or)  $[N_{1114}]Br$  and sodium dodecylbenzenesulfonate ( $[\text{Na}]DBS$ ) were dissolved in dichloromethane (DCM) and stirred for 24 h at room temperature. The precipitated NaBr was filtered with Whatmann filter paper. The DCM layer was washed with water several times to completely remove  $\text{Br}^-$  ions present. The washing was performed until the aqueous layer gives a clear solution even with the addition of excess 1 M  $\text{AgNO}_3$ . The DCM layer was then dried over  $\text{Na}_2\text{SO}_4$  followed by removal of solvent. Thus, obtained DBS-ILs were dried for several hours under vacuum and stored in a desiccator prior to use. All DBS-ILs were characterized by LC–MS  $^1\text{H}$  NMR techniques and elemental analysis. Molecular structures of the cations and anions of the synthesized DBS-ILs are given in Figure 1.

$^1\text{H}$  NMR Chemical Shift Data. (1)  $[C_4\text{Py}]DBS$ .  $^1\text{H}$  NMR 200 MHz (DMSO- $d_6$ ):  $\delta_{\text{H}}$  (ppm) 9.132 (d, 2H), 8.605 (t, 1H), 8.156 (t, 2H), 7.553 (d, 2H), 7.282 (2H), 4.610 (t, 2H), 2.505 (S, 1H), 1.883 (q, 2H), 1.524 (m, 4H), 1.236 (m, 10H), 0.893 (m, 5H), 0.772 (m, 12H). ESI-MS:  $[\text{C}_9\text{H}_{14}\text{N}]^+$   $m/z$  136.21,  $[\text{C}_{18}\text{H}_{29}\text{O}_3\text{S}]^-$   $m/z$  325.49

(2)  $[C_4\text{mim}]DBS$ .  $^1\text{H}$  NMR 200 MHz (DMSO- $d_6$ ):  $\delta_{\text{H}}$  (ppm) 9.122 (s, 1H), 7.769 (d, 2H), 7.528 (d, 2H), 7.277 (m, 2H), 4.153 (t, 2H), 3.842 (s, 3H), 1.755 (q, 2H), 1.525 (m, 3H), 1.235 (m, 14H), 0.801 (m, 17H). ESI-MS:  $[\text{C}_8\text{H}_{15}\text{N}]^+$   $m/z$  139.22,  $[\text{C}_{18}\text{H}_{29}\text{O}_3\text{S}]^-$   $m/z$  325.50

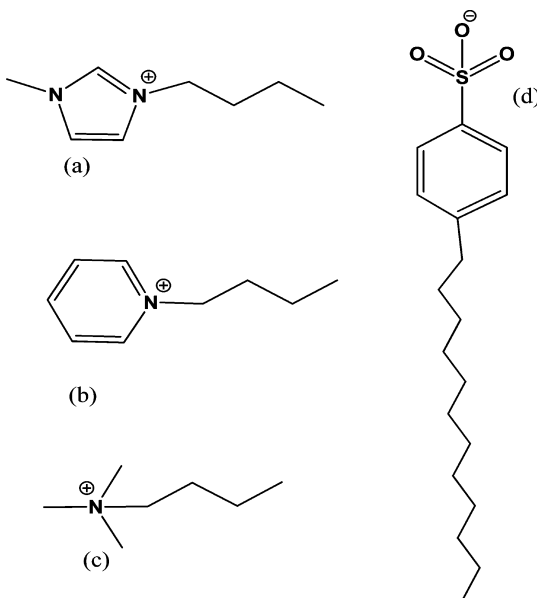


**Figure 1.** Molecular structures of the cations and anions of synthesized DBS-ILs: (a)  $[\text{C}_4\text{mim}]^+$ ; (b)  $[\text{C}_4\text{Py}]^+$ ; (c)  $[\text{N}_{1114}]^+$ ; and (d)  $[\text{DBS}]^-$ .

(3)  $[\text{N}_{1114}]\text{DBS}$ .  $^1\text{H}$  NMR 200 MHz ( $\text{D}_2\text{O}$ ):  $\delta_{\text{H}}$  (ppm) 7.592 (d, 2H), 7.227 (d, 2H), 3.024 (t, 2H), 2.869 (s, 9H), 1.429 (m, 5H), 1.077 (m, 13H), 0.654 (m, 15H). ESI-MS:  $[\text{C}_7\text{H}_{18}\text{N}]^+ m/z$  116.10,  $[\text{C}_{18}\text{H}_{29}\text{O}_3\text{S}]^- m/z = 325.47$

**2.3. Methods.** 2.3.1. *Tensiometry.* Surface tension measurements were carried out at 298.15 K using a Data Physics DCAT-II automated Tensiometer employing the Wilhelmy plate method. Aliquots of DBS-IL stock solutions

were added to Millipore grade water by volume and stirred for about 10 min for complete solubilization. Prior to measurements, the resultant solutions were kept for at least 10 min for equilibration. The data were collected in triplicate and found to be accurate within  $\pm 0.1 \text{ mN}\cdot\text{m}^{-1}$ . The temperature of the measurement cell was controlled with a Julabo water thermostat to within 0.1 K.

**2.3.2. Conductometry.** Specific conductivity was measured by a digital conductivity meter (Systronics 308) using a cell with a unit cell constant. The temperature of the measurement cell was controlled with a Julabo water thermostat to within 0.1 K. The conductivity was measured after each aliquot addition of DBS-IL stock solution to a conductivity cell containing Millipore water. Measurements were performed with an uncertainty of less than 0.5%.

**2.3.3. Isothermal Titration Calorimetry (ITC).** Calorimetric titration was performed with a MicroCal ITC200 microcalorimeter. The sample and reference cells were filled with Millipore water and stabilized at 298.15 K. Amounts of 40  $\mu\text{L}$  of DBS-IL stock solutions prepared in water were taken in an instrument-controlled Hamiltonian syringe, and 2  $\mu\text{L}$  aliquots were added to the sample cell containing 200  $\mu\text{L}$  of water with continuous stirring (500 rpm). The parameters like time of addition and duration between each addition were controlled by software provided with the instrument. The enthalpy change at each injection was measured and plotted against concentration by using origin software provided with the instrument.

**2.3.4. Dynamic Light Scattering (DLS).** DLS measurements were performed at 298.15 K by using a NaBiTec SpectroSize300 light-scattering apparatus (NaBiTec, Germany) with a He–Ne laser (633 nm, 4 mW). DBS-IL solutions of a concentration above the CMC were filtered directly into the

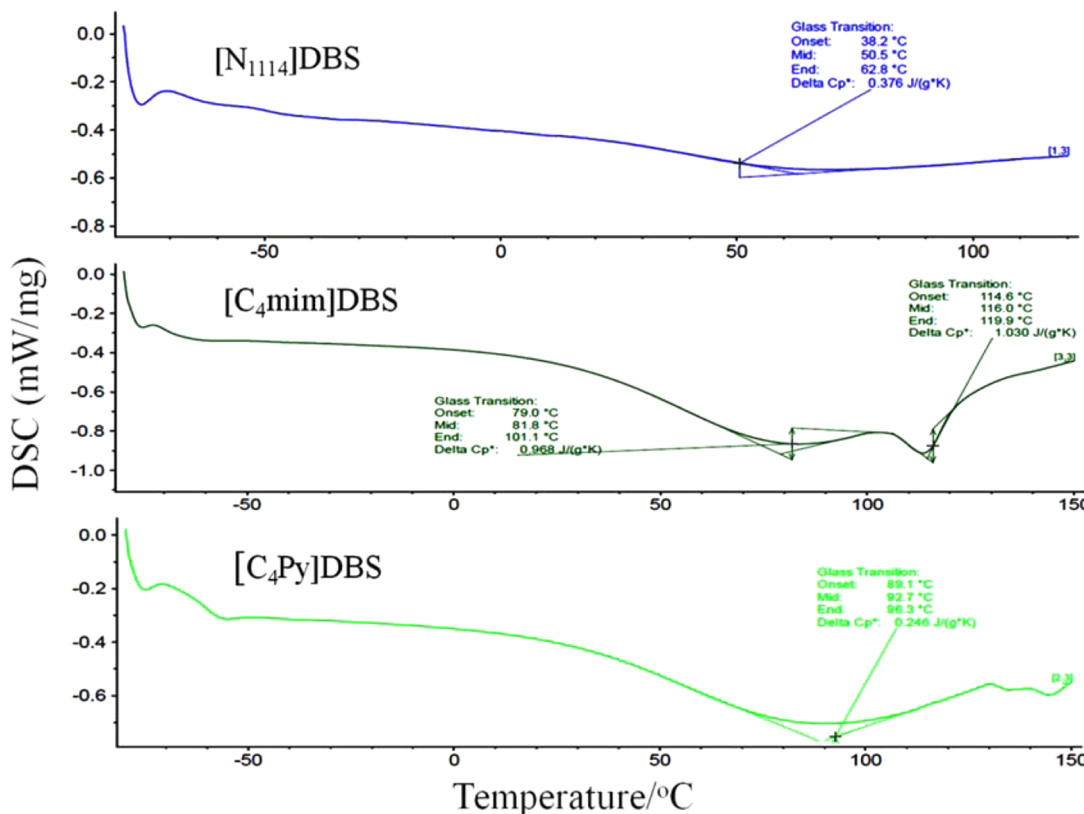


**Figure 2.** DSC thermograms of DBS-ILs showing melting points below 100 °C.

quartz cell using a membrane filter of  $0.45\text{ }\mu\text{m}$  pore size. Prior to measurements, the quartz cell was rinsed several times with filtered water and then filled with filtered sample solutions. The temperature of the measurements was controlled with an accuracy of  $0.1\text{ K}$ . The data evaluation of the dynamic light-scattering measurements was performed with the inbuilt CONTIN algorithm.

**2.3.5. Cryo-Transmission Electron Microscopy (cryo-TEM).** For cryogenic transmission electron microscopy (cryo-TEM) studies, a drop of the sample was put onto a lacey TEM grid, where most of the liquid was removed with blotting paper, leaving a thin film stretched over the lace. The specimens were instantly vitrified by rapid immersion into liquid ethane and cooled to approximately  $90\text{ K}$  by liquid nitrogen in a temperature-controlled freezing unit (Zeiss Cryobox, Zeiss NTS GmbH, Oberkochen, Germany). The temperature was monitored and kept constant in the chamber during all of the sample preparation steps. Afterward, the specimen was inserted into a cryo-transfer holder (CT3500, Gatan, München, Germany) and transferred to a Zeiss EM922 EF-TEM instrument. Examinations were carried out at temperatures of around  $90\text{ K}$ . The transmission electron microscope was operated at an acceleration voltage of  $200\text{ kV}$ . All images were registered digitally by a bottom-mounted CCD camera system (Ultrascan 1000, Gatan) combined and processed with a digital imaging processing system (Gatan Digital Micrograph 1.8).

**2.3.6.  $^1\text{H}$  NMR and  $^1\text{H}$ - $^1\text{H}$  2D-NOESY Measurements.** The  $^1\text{H}$  NMR spectra of synthesized DBS-ILs were recorded in DMSO and  $\text{D}_2\text{O}$  using a Brüker 200 MHz spectrometer. The  $^1\text{H}$  NMR spectra of  $[\text{Na}]$ DBS and DBS-ILs were recorded at  $10\text{ mM}$  concentration in  $\text{D}_2\text{O}$  and  $100\text{ mM}$  NaBr solution in  $\text{D}_2\text{O}$  using a Brüker 200 MHz spectrometer. Phase-sensitive  $^1\text{H}$ - $^1\text{H}$  2D-NOESY NMR experiments were acquired with 48 numbers of scan and  $720\text{ ms}$  mixing time and processed through Topspin software. The mixing time used for the NOESY experiment was optimized through an inversion recovery method. 2D-NOESY NMR experiments were recorded using a Brüker 500 MHz spectrometer.

**2.3.7. Viscometry, Turbidimetry, and Refractive Index Measurements.** The viscosity, turbidity, and refractive index of colloidal solutions of  $[\text{Na}]$ DBS and DBS-ILs were measured at  $298.15\text{ K}$  on a Brookfield viscometer (Synchroelectric Viscometer, Stoughton, MA02072, USA) using spindle No. 1 at  $100\text{ rpm}$ , Eutech Instruments Turbidimeter, and a digital refractometer (Mettler Toledo RE40D refractometer), respectively. Prior to measurements the solutions were allowed to equilibrate overnight after homogeneous mixing, and measurements were taken in triplicate.

### 3. RESULTS AND DISCUSSION

**3.1. Melting Points of DBS-ILs.** The melting point of  $[\text{Na}]$ DBS is above  $300\text{ }^\circ\text{C}$  which decreased significantly to less than  $100\text{ }^\circ\text{C}$  by replacing a sodium counterion with large organic counterions, viz., *n*-butyltrimethylammonium, *N*-butylpyridinium, and 1-butyl-3-methylimidazolium. The melting points for DBS-ILs measured from DSC were found to be  $50.5$ ,  $81.8$ , and  $92.7\text{ }^\circ\text{C}$  for  $[\text{N}_{1114}]$ DBS,  $[\text{C}_4\text{mim}]$ DBS, and  $[\text{C}_4\text{Py}]$ DBS, respectively (DSC thermograms are provided in Figure 2). Since ILs are typically regarded as salts with melting points below  $100\text{ }^\circ\text{C}$ , these DBS-ILs can be considered as surface-active ionic liquids (SAILs). The replacement of the sodium counterion of conventional surfactant  $[\text{Na}]$ DBS

disrupts the efficient packing and decreases the lattice energy, consequently leading to a drop in melting point, thus forming ILs.

**3.2. Surface Tension.** Surface tension  $\gamma$  of  $[\text{Na}]$ DBS and DBS-ILs as a function of concentration in aqueous solutions at  $25\text{ }^\circ\text{C}$  were measured to establish their critical micelle concentration (CMC) and generate adsorption parameters (Figure 3 and Table 1). The CMCs for DBS-ILs were found to

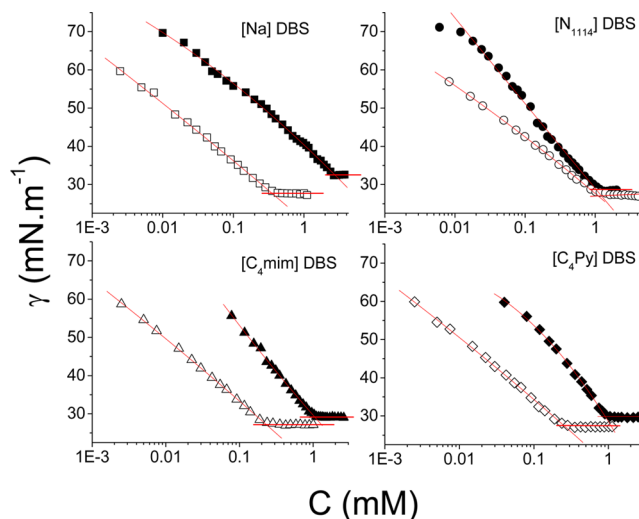


**Figure 3.** Decrease in surface tension of water with the addition of  $[\text{Na}]$ DBS or DBS-ILs (fill symbols) in pure water or (hollow symbols) in  $100\text{ mM}$  aqueous sodium bromide.

be lower than their conventional analogue  $[\text{Na}]$ DBS. This decrease in CMC may be because of replacement of a more hydrated  $\text{Na}^+$  ion with the less hydrated and hydrophobic large organic counterions ( $[\text{N}_{1114}]$ ,  $[\text{C}_4\text{mim}]$ ,  $[\text{C}_4\text{Py}]$ ) which are more effective in screening like charge electrostatic repulsions between surface-active anions at the air–water interface, thereby decreasing the free energy of micellization. The order of CMC was found as  $[\text{C}_4\text{Py}]$ DBS  $< [\text{C}_4\text{mim}]$ DBS  $< [\text{N}_{1114}]$ DBS  $< [\text{Na}]$ DBS. Addition of NaBr further decreased the CMCs of  $[\text{Na}]$ DBS and DBS-ILs with order of CMC as  $[\text{C}_4\text{py}]$ DBS  $\sim$   $[\text{C}_4\text{mim}]$ DBS  $< [\text{Na}]$ DBS  $< [\text{N}_{1114}]$ DBS.

The effectiveness of these DBS-ILs at reducing limiting surface tension ( $\gamma_{\text{CMC}}$ ) is very interesting. In the absence of NaBr the DBS-ILs have shown lower  $\gamma$  values than their conventional analogue  $[\text{Na}]$ DBS, similar to the other anionic surface active ionic liquids.<sup>28,32</sup> The  $\gamma_{\text{CMC}}$  of  $[\text{C}_4\text{mim}]$ DBS ( $29.18\text{ mN}\cdot\text{m}^{-1}$ ) is lower than their analogous single-chain anionic SAIL having a dodecylsulfate anion  $[\text{C}_4\text{mim}]$ DS ( $34.4\text{ mN}\cdot\text{m}^{-1}$ ).<sup>35,26</sup> This is due to the higher hydrophobicity of the DBS anion because of the presence of a benzene ring in the molecule. The  $\gamma_{\text{CMC}}$  for  $[\text{Na}]$ DBS and DBS-ILs in aqueous medium is also significantly reduced in the presence of NaBr (Table 1). Interestingly in the presence of NaBr,  $[\text{Na}]$ DBS and DBS-ILs have shown equal efficiency for reducing limiting surface tension ( $\sim 27\text{ mN}\cdot\text{m}^{-1}$ ).

The adsorption efficiency of DBS-ILs at the air–water interface is estimated by measuring  $pC_{20}$  using the relation<sup>1,59</sup>

$$pC_{20} = -\log C_{20} \quad (1)$$

where,  $C_{20}$  is the concentration needed to reduce the surface tension of the solvent (water in the present case) by  $20\text{ mN}\cdot\text{m}^{-1}$ . The higher  $pC_{20}$  value indicates high adsorption efficiency

**Table 1.** Critical Micelle Concentration (CMC), Surface Tension at CMC ( $\gamma_{\text{CMC}}$ ), Effective Surface Tension Reduction ( $\pi_{\text{CMC}}$ ), Adsorption Efficiency ( $pC_{20}$ ), Maximum Surface Excess Concentration ( $\Gamma_{\text{max}}$ ), and Area Occupied by a Single Molecule at the Air–Water Interface ( $A_{\text{min}}$ ) of DSB-ILs in Aqueous and 100 mM Aqueous NaBr Medium at 298.15 K

surfactant/SAIL	CMC (mM)		$\gamma_{\text{CMC}}$ (mN·m <sup>-1</sup> )		$\pi_{\text{CMC}}$ (mN·m <sup>-1</sup> )		$pC_{20}$		$\Gamma_{\text{max}}$ (μmol·m <sup>-2</sup> )		$A_{\text{min}}$ (Å <sup>2</sup> )	
	water	aq.NaBr	water	aq.NaBr	water	aq.NaBr	water	aq.NaBr	water	aq.NaBr	water	aq.NaBr
[Na]DBS	2.75	0.38	32.49	27.7	39.51	44.30	3.71	5.06	1.54	1.37	108.34	121.67
[N <sub>1114</sub> ]DBS	1.34	1.06	29.11	27.44	42.89	44.56	3.89	4.72	2.21	1.23	75.57	135.23
[C <sub>4</sub> mim]DBS	1.08	0.25	29.18	27.11	42.82	44.89	3.94	5.15	2.09	1.47	79.86	113.27
[C <sub>4</sub> Py]DBS	0.92	0.26	29.69	27.15	42.31	44.85	3.92	5.10	2.31	1.43	72.08	116.69

of the surfactant.<sup>26</sup> The  $pC_{20}$  values obtained for DBS-ILs in aqueous medium are higher than [Na]DBS, and the value obtained for [C<sub>4</sub>mim]DBS (3.94) is higher than the analogous SAILS [C<sub>4</sub>mim]DS (3.3).<sup>35</sup> The presence of NaBr improved the adsorption efficiency of all four surfactants tremendously, and the values obtained for single-chain [Na]DBS/DBS-ILs (~5.2) are higher than double-chain SAILS (AOT-ILs)<sup>32</sup> (~4.4). Effectiveness of surface tension reduction is the other parameter that measures the adsorption efficiency of a surfactant, denoted by  $\pi_{\text{CMC}}$  and calculated using the relation 2.

$$\pi_{\text{CMC}} = \gamma_0 - \gamma_{\text{CMC}} \quad (2)$$

where  $\gamma_0$  stands for the surface tension of the pure solvent, and  $\gamma_{\text{CMC}}$  stands for the surface tension of the solvent medium at CMC. The values obtained for  $\pi_{\text{CMC}}$  and  $pC_{20}$  indicate the higher adsorption efficiency of DBS-ILs than its conventional analogue [Na]DBS which further increased with the addition of NaBr. Due to the bigger size, the cations of DBS-ILs experience less hydration and populate in higher number at the interface as compared to the highly hydrating sodium ion, thus increasing their adsorption efficiency. With the addition of electrolyte the adsorption efficiency of both [Na]DBS and DBS-ILs at the air–water interface improved tremendously, and the adsorption efficiency is observed to be higher than double-chain surfactant/SAILS.

The amount of DBS-ILs adsorbed at the interface is estimated by deriving surface excess concentration ( $\Gamma_{\text{max}}$ ) using Gibbs adsorption (eq 3) that allowed the estimation of a minimum area occupied by DBS-ILs at the interface ( $A_{\text{min}}$ ) using eq 4

$$\Gamma_{\text{max}} = -\frac{1}{nRT} \frac{\partial \gamma}{\partial \ln C} \quad (3)$$

$$A_{\text{min}} = \frac{1}{\Gamma_{\text{max}} N_A} \quad (4)$$

where “ $\partial \gamma / \partial \ln C$ ” is the slope of the  $\gamma - \ln C$  plot in the pre-CMC region;  $N_A$  is Avogadro number; and  $n$  is the prefactor, taken as 2 for all DBS-ILs by considering 1:1 dissociation in aqueous medium.<sup>60</sup> The concentration just below the CMC is considered to obtain  $\Gamma_{\text{max}}$  from which it is possible to obtain the  $A_{\text{min}}$  value at near saturation of the interface. The  $A_{\text{min}}$  value obtained for DBS-ILs is lower than that of [Na]DBS in pure aqueous medium; however, in the presence of electrolyte the value is higher for all the surfactant/SAILS. Further, in the presence of electrolyte  $A_{\text{min}}$  is lower for [C<sub>4</sub>mim]DBS and [C<sub>4</sub>Py]DBS than [N<sub>1114</sub>]DBS and [Na]DBS (Table 1).

**3.3. Isothermal Titration Calorimetry (ITC).** The  $\Delta H_{\text{dil}}$  is endothermic, whereas  $\Delta H_{\text{mic}}$  is exothermic for DBS-ILs and [Na]DBS both in pure water and in the presence of 100 mM NaBr (Figures 4 and 5). It is interesting to note that the plateau after CMC in these enthalpograms does not stay flat. All the

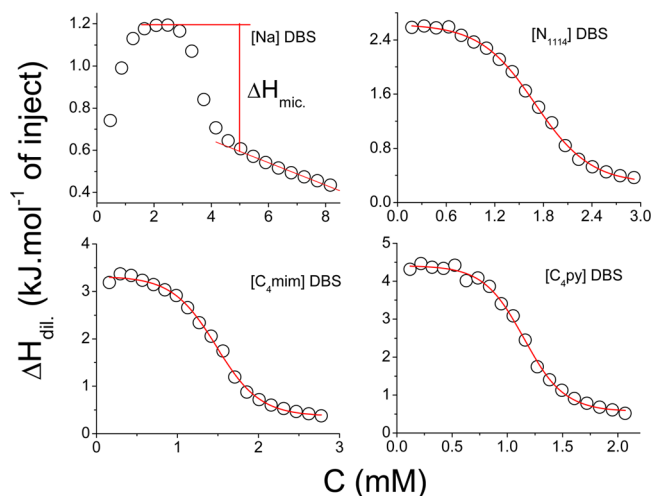


**Figure 4.** Enthalpograms of [Na]DBS and DBS-ILs in pure aqueous medium at 298.15 K.

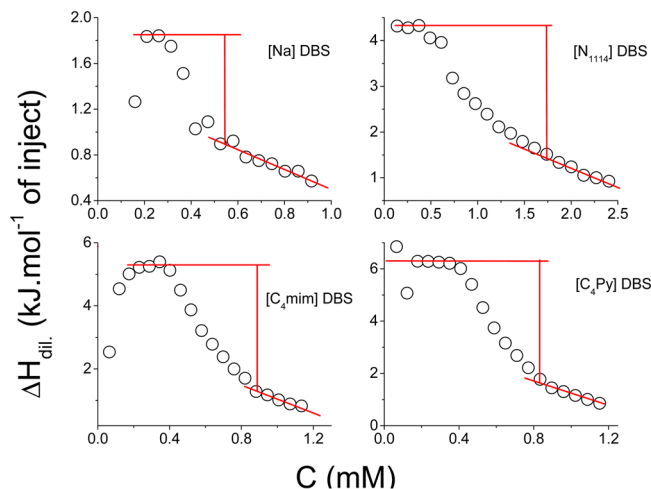


**Figure 5.** Enthalpograms of [Na]DBS and DBS-ILs in aqueous medium in the presence of 100 mM sodium bromide at 298.15 K.

enthalpograms exhibit a positive slope after CMC unlike in dodecylsulfate-based SAILS where a sharp change at CMC in  $\Delta H_{\text{dil}}$  is observed.<sup>35</sup> As noted from surface tension measurements, the CMC of DBS-ILs is lower than the CMC of [Na]DBS which further reduced with the addition of electrolyte NaBr. The CMC values obtained from ITC are slightly higher than those obtained from surface tension measurements. This is normally due to the slow process of micellization of [Na]DBS and DBS-ILs as shown in Figure 3 since surface tension measures the saturation of the air–water interface as CMC and ITC measures the formation of the micelle as CMC. However, the order of CMC for all the compounds is the same from both

**Table 2.** Critical Micelle Concentration (CMC), Standard Enthalpy of Micellization ( $\Delta H_{\text{mic}}^{\circ}$ ), Standard Gibb's Free Energy of Micellization ( $\Delta G_{\text{mic}}^{\circ}$ ), and Standard Entropy of Micellization ( $\Delta S_{\text{mic}}^{\circ}$ ) of DBS-ILs and [Na]DBS in Aqueous and 100 mM Aqueous NaBr Media at 298.15 K

surfactant/SAIL	CMC (mM)		$\Delta H_{\text{mic}}^{\circ}$ (kJ·mol <sup>-1</sup> )		$\Delta G_{\text{mic}}^{\circ}$ (kJ·mol <sup>-1</sup> )		$\Delta S_{\text{mic}}^{\circ}$ (J·mol <sup>-1</sup> )	
	water	aq. NaBr	water	aq. NaBr	water	aq. NaBr	water	aq. NaBr
[Na]DBS	3.74	0.37	-0.62	-1.04	-30.04	-37.28	98.69	121.55
[N <sub>1114</sub> ]DBS	1.90	0.73	-1.70	-2.95	-33.67	-36.80	107.23	113.55
[C <sub>4</sub> mim]DBS	1.47	0.52	-2.79	-3.97	-34.95	-38.39	107.87	115.47
[C <sub>4</sub> Py]DBS	1.16	0.53	-3.51	-4.51	-36.07	-38.69	109.21	114.65

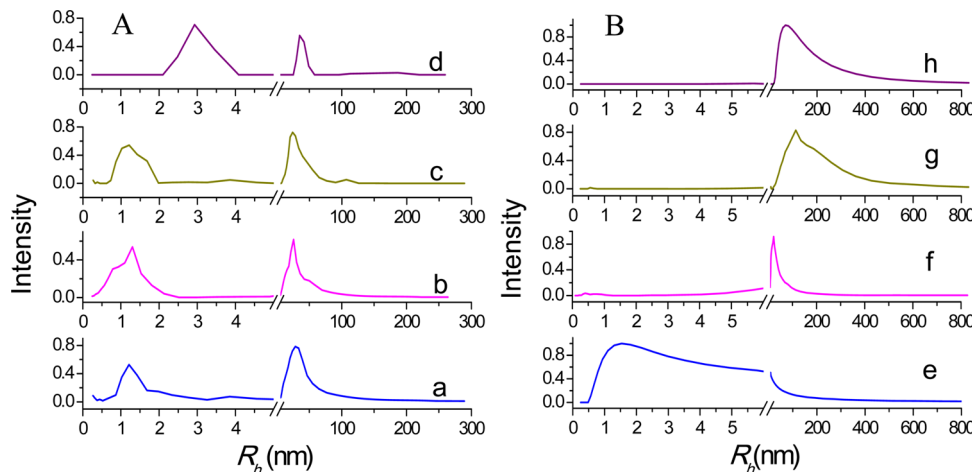


**Figure 6.** DLS size distributions of 10 mM [Na]DBS and DBS-ILs in (A) pure aqueous medium and (B) in 100 mM aqueous sodium bromide medium. (a, e) [Na]DBS; (b, f) [N<sub>1114</sub>]DBS; (c, g) [C<sub>4</sub>mim]DBS; (d, h) [C<sub>4</sub>Py]DBS.

the techniques (Table 2). Using the ITC determined CMC and  $\Delta H_{\text{mic}}$  values,  $\Delta G_{\text{mic}}$  and  $\Delta S_{\text{mic}}$  were calculated using eqs 5 and 6

$$\Delta G_{\text{mic}} = (1 + \beta)RT \ln X_{\text{CMC}} \quad (5)$$

$$\Delta S_{\text{mic}} = \frac{\Delta H_{\text{mic}} - \Delta G_{\text{mic}}}{T} \quad (6)$$

where  $\beta = (1 - \alpha)$  is the counterion binding calculated from the degree of dissociation “ $\alpha$ ” value estimated from the conductivity measurements by measuring the ratio of the slope of the lines before and after the transition point from specific conductivity versus concentration graphs (Supporting Information Figure S1). As  $\beta$  values could not be obtained for aqueous electrolyte systems because of large fluctuations in conductivity measurements as a consequence of higher ionic strength of the medium, the values of  $\beta$  obtained in aqueous medium are used for the calculation of  $\Delta G_{\text{mic}}$  in aqueous NaBr medium (the actual  $\beta$  values in the case of aqueous electrolyte solutions are normally higher because of increased degree of counterion binding). All the thermodynamic parameter values obtained in this study are given in Table 2. The negative  $\Delta G_{\text{mic}}$  in all the cases indicates spontaneous micellization. In the presence of NaBr,  $\Delta G_{\text{mic}}$  becomes more negative indicating the improved efficiency of SAILs in the presence of electrolyte. The values obtained for  $\Delta H_{\text{mic}}$  are negative in all cases indicating exothermic changes due to micellization. All the values obtained for  $\Delta S_{\text{mic}}$  are positive in all cases, and the values are higher in the presence of NaBr. These thermodynamic parameters indicate that the process of micellization for [Na]DBS and DBS-ILs is primarily entropy driven in both aqueous and aqueous NaBr medium.

### 3.4. Characterization of Self-Assembled Structures.

Dynamic light scattering (DLS), turbidity, cryo-TEM, and <sup>1</sup>H NMR measurements were performed to determine the size, shape, and type of the self-assembled structures of [Na]DBS and DBS-ILs in aqueous medium in the absence and presence of NaBr. The hydrodynamic radii,  $R_h$ , of the self-assembled structures measured from DLS are shown in Figure 6(A, B). DLS results show dual distributions in pure aqueous medium at a concentration of 10 mM for both [Na]DBS and DBS-ILs, one at  $R_h \sim 4$  nm (typical micelle region) and the other one at  $R_h \sim 100$  nm (typical vesicle region). DLS measurements are also performed at different concentrations of [Na]DBS and DBS-ILs above the CMC, i.e., at 4, 10, 40, 60, and 100 mM, to examine the concentration-dependent changes in size distribution, where no significant changes are observed indicating the similar solution structures at all concentrations (DLS size distributions are given in Supporting Information Figure S2). Since [Na]DBS and DBS-ILs behaved in a similar way at all concentrations, we have chosen 10 mM solutions for further studies about the self-assembled structures in the presence of electrolyte. In the presence of 100 mM NaBr the DLS results showed a single distribution of hydrodynamic radius,  $R_h \sim 4$  nm for [Na]DBS and  $R_h \sim 60$  nm for DBS-ILs, micelle formation by [Na]DBS, and vesicle formation by DBS-ILs unlike in pure aqueous medium. To optimize the minimum concentration needed to induce MVT in DBS-ILs, DLS measurements were performed at 10 mM concentration of [Na]DBS and DBS-ILs at varying concentrations of NaBr in aqueous medium. The obtained size distributions at varying salt concentrations are provided in the Supporting Information (Figure S3). Turbidity measurements have further supported the MVT. The turbidity experiments performed at 10 mM

concentration of  $[Na]DBS$  and DBS-ILs at increasing NaBr concentration have shown a slope increase after reaching 60 mM concentration for DBS-ILs, whereas  $[Na]DBS$  has not shown any sign of turbidity even at 100 mM NaBr concentration (Figure 7). In the solutions of DBS-ILs turbidity

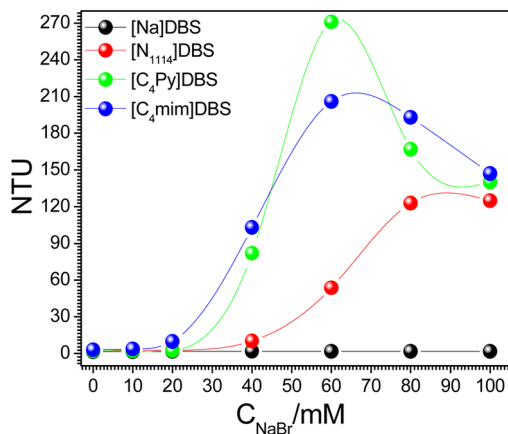


**Figure 7.** Change in turbidity of colloidal solutions of 10 mM  $[Na]DBS$  and DBS-ILs at varying concentrations of sodium bromide in aqueous media.

increases due to formation of vesicles, whereas in the case of  $[Na]DBS$  solution no change in turbidity was observed indicating the formation of micelles only.

The self-assembled structures were further confirmed from cryo-TEM experiments (Figure 8). Images were recorded for the solutions containing 10 mM concentration of either  $[Na]DBS$  or a representative DBS-IL,  $[C_4mim]DBS$ , in aqueous and 100 mM NaBr solution. Since all three DBS-ILs showed similar behavior in DLS, we carried out cryo-TEM imaging of only  $[C_4mim]DBS$ . In the aqueous medium, cryo-TEM images suggested the existence of micelles along with some loose aggregates (low contrast) in the case of  $[Na]DBS$  and predominantly the micelles along with only some vesicular structures in  $[C_4mim]DBS$  as shown in Figure 8D. The cryo-TEM images of  $[C_4mim]DBS$  in 100 mM aqueous NaBr solution suggested the formation of unilamellar vesicles (Figure 8E) along with some multilamellar vesicles (Figure 8F). Thus, both the DLS and cryo-TEM experiments suggested the salt-induced vesicle formation by DBS-ILs in aqueous medium which otherwise forms micelles predominantly. The formation of compact and higher self-assembled structures, like vesicles, leads to peak broadening because of restricted movement and shorter relaxation times of nuclei.<sup>61</sup> Therefore, <sup>1</sup>H NMR spectra of aqueous solutions of DBS-ILs and  $[Na]DBS$  were recorded at 10 mM concentration in pure aqueous medium and in the presence of 100 mM NaBr. The changes in the peak broadening of DBS-ILs in pure water and 100 mM NaBr solution are shown in Figure 9. The peak broadening in electrolyte solutions arises due to the formation of higher self-assembled structures such as vesicles, whereas the peaks at the same concentration in pure aqueous medium are sharp, suggesting the presence of micelles. The <sup>1</sup>H NMR spectra of  $[Na]DBS$  remain sharp in aqueous electrolyte medium, similar to the aqueous medium suggesting the existence of micelles in both the media.

### 3.5. Mechanism of Micelle to Vesicle Transition (MVT) upon Addition of NaBr.

Cation– $\pi$  or  $\pi$ – $\pi$  interactions are widely present between an electron-rich  $\pi$  system (aromatic

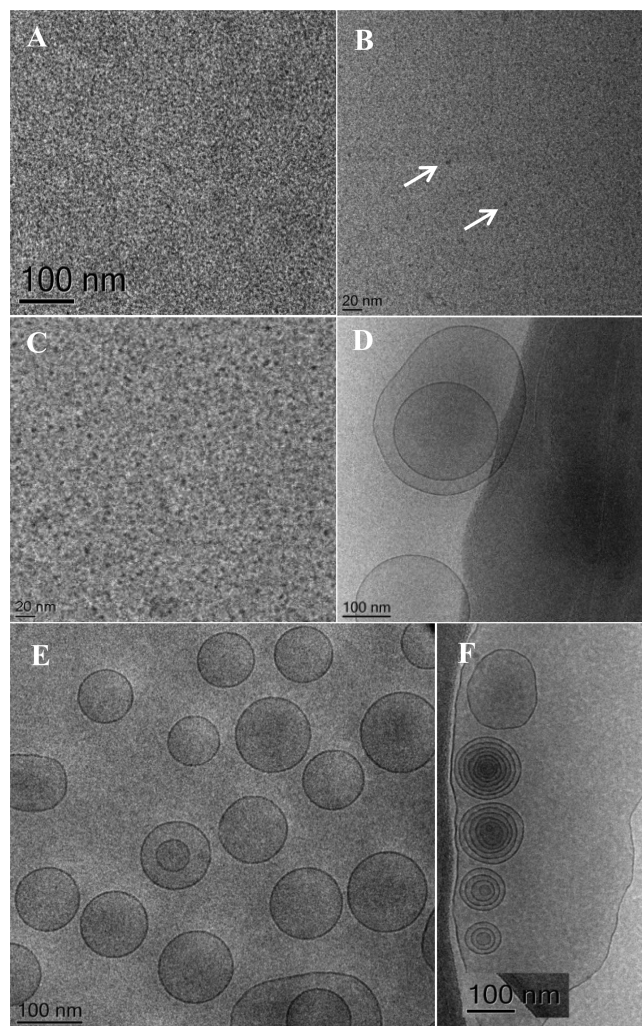


**Figure 8.** (A,B) Cryo-TEM images of micelles of  $[Na]DBS$  in water and 100 mM aqueous sodium bromide solution; (C, D) micelles and unilamellar vesicles of  $[C_4mim]DBS$  in water; and (E, F) unilamellar and multilamellar vesicles of  $[C_4mim]DBS$  in 100 mM aqueous sodium bromide solution.

ring) and adjacent cations or another electron-rich  $\pi$  system.<sup>62</sup> In aqueous solution these kinds of interactions are even more strong than electrostatic interactions because of low desolvation penalty.<sup>63</sup> SFA measurements and theoretical simulations have shown that monovalent cation– $\pi$  or  $\pi$ – $\pi$  interactions mainly depend upon the degree of hydration of species involved<sup>64</sup> and are comparatively higher for less hydrated and large-sized hydrophobic ions such as *n*-butyltrimethylammonium, 1-butyl-3-methylimidazolium, or 1-butylpyridinium and dodecylbenzenesulfonate investigated herein. Besides hydration, these interactions are highly orientation dependent, and the orientation sensitivity of cations or the electron-rich  $\pi$  system can significantly increase or decrease their efficiency.<sup>65</sup> Addition of NaBr to DBS-IL micellar systems not only enhances the surfactant adsorption efficiency by causing the newly adsorbed surfactant molecules to adopt a vertical orientation at the air–water interface<sup>58</sup> but also reduces the hydration of the benzenesulfonate headgroup and counterions by causing the change in water network. Thus, the increased electrostatic interactions and favorable orientations resulting in cation– $\pi$  interactions between *n*-butyltrimethylammonium and dodecylbenzenesulfonate or  $\pi$ – $\pi$  interactions between 1-butyl-3-

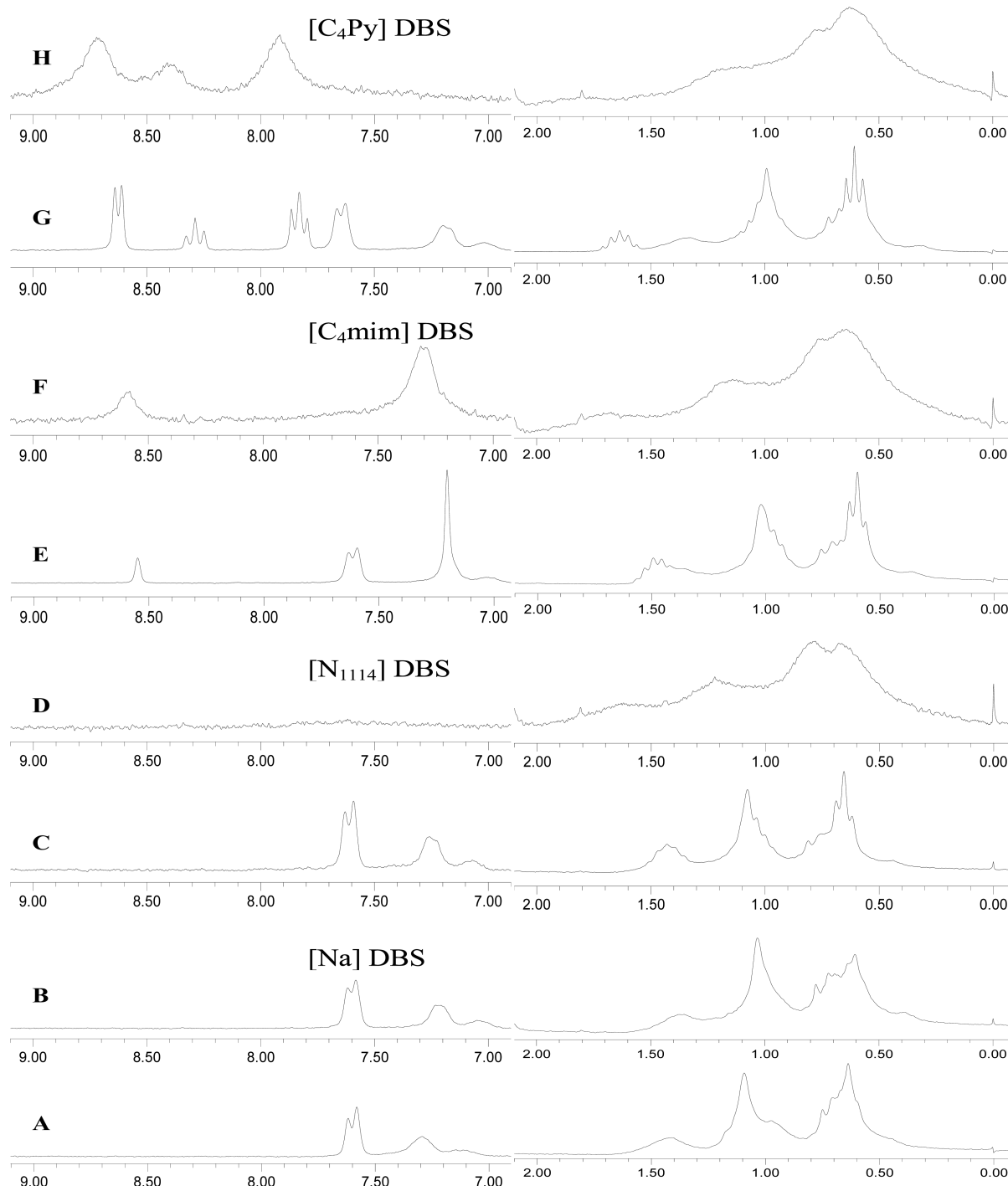


**Figure 9.** NMR spectra of 10 mM [Na]DBS and DBS-ILs in deuterated aqueous and aqueous sodium bromide medium. (A), (C), (E), and (G) are [Na]DBS, [N<sub>1114</sub>]DBS, [C<sub>4</sub>mim]DBS, and [C<sub>4</sub>Py]DBS, respectively, in pure aqueous medium where (B), (D), (F), and (H) are [Na]DBS, [N<sub>1114</sub>]DBS, [C<sub>4</sub>mim]DBS, and [C<sub>4</sub>Py]DBS, respectively, in 100 mM aqueous sodium bromide medium.

methylimidazolium or 1-butylpyridinium and dodecylbenzenesulfonate as a consequence of addition of NaBr leads to MVT.

Evidence of  $\pi-\pi$  interactions between the headgroup and counterions and arrangement of cations and anions in a vesicle at 100 mM NaBr concentration has been collected from NOESY NMR spectroscopy (schematic representation is shown in Figure 10). The NOESY NMR spectra of the [C<sub>4</sub>mim]DBS and [C<sub>4</sub>Py]DBS (Figure 11 and Figure 12 respectively) show strong NOEs originating from intermolecular interactions between the protons of aromatic head groups

(imidazolium/pyridinium-benzene of DBS) and from intermolecular interactions between the protons of the aliphatic chains of both (butyl and dodecyl chain). In Figure 11A (expanded form) the NOE cross peak obtained corresponds to the alkyl chain of the butyl and dodecyl group (8H) suggesting that both the alkyl chains are parallel. In Figure 11B (expanded form with water suppressing the 1D external projection representing the invisible peak of the aromatic region for a better understanding) aromatic protons of the imidzolium headgroup (1H, 2H, 3H) show weak NOE with aromatic

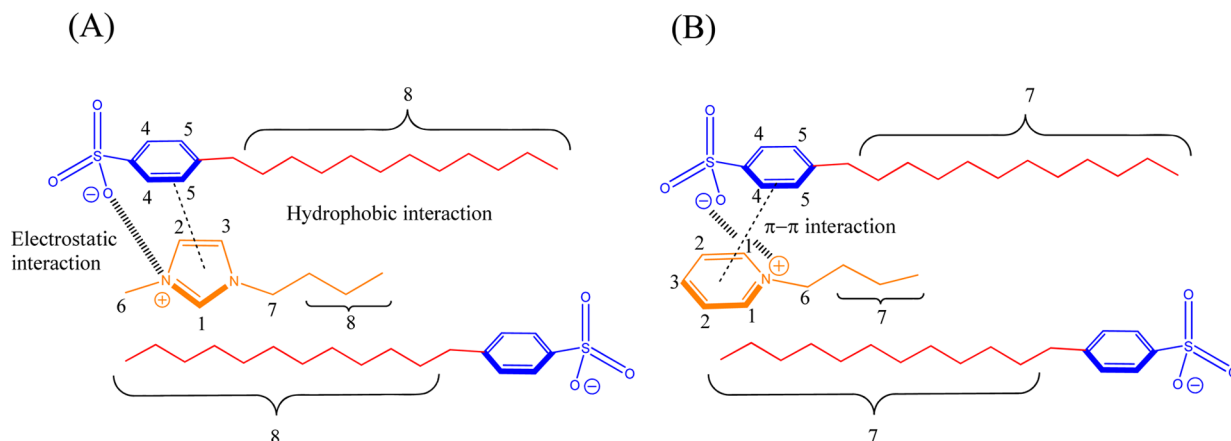


**Figure 10.** Scheme representing peak positions and possible interactions in vesicular structures of (A)  $[C_4\text{mim}]$ DBS and (B)  $[C_4\text{Py}]$ DBS.

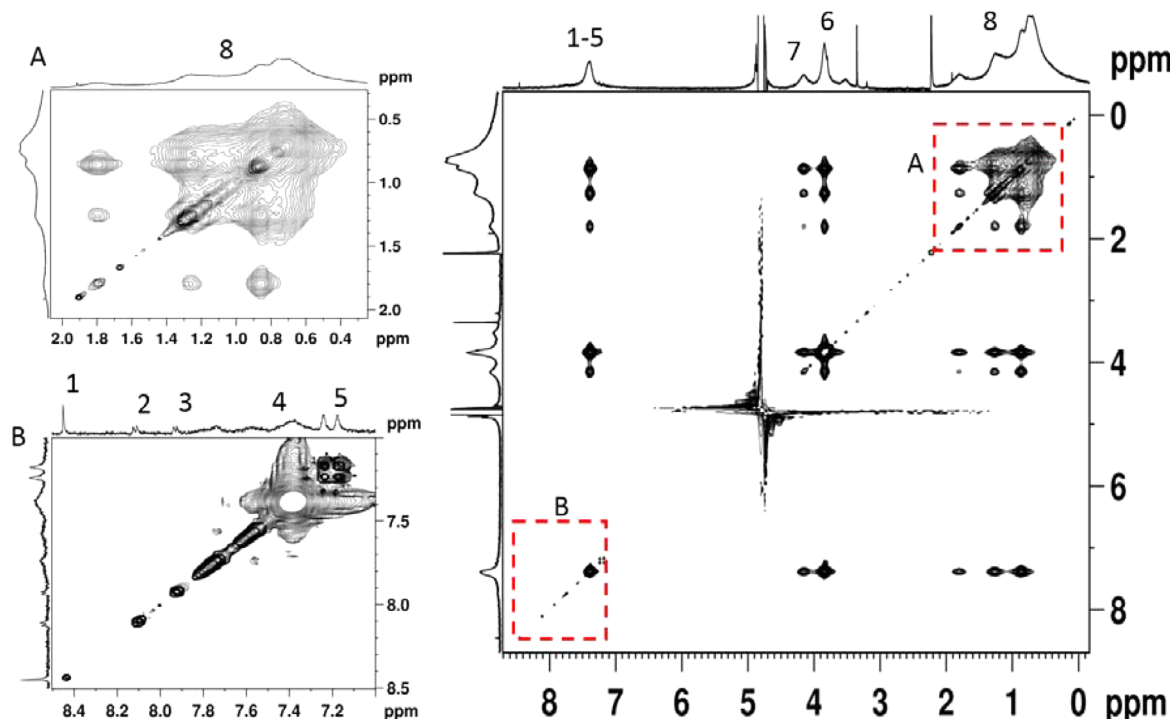


**Figure 11.** NOESY spectrum of  $[C_4\text{mim}]$ DBS in deuterated 100 mM NaBr solution. These NOEs originate from interaction between (A) the alkyl chain proton of both the butyl and dodecyl group and (B) aromatic proton (DBS) interactions with the imidazolium proton.

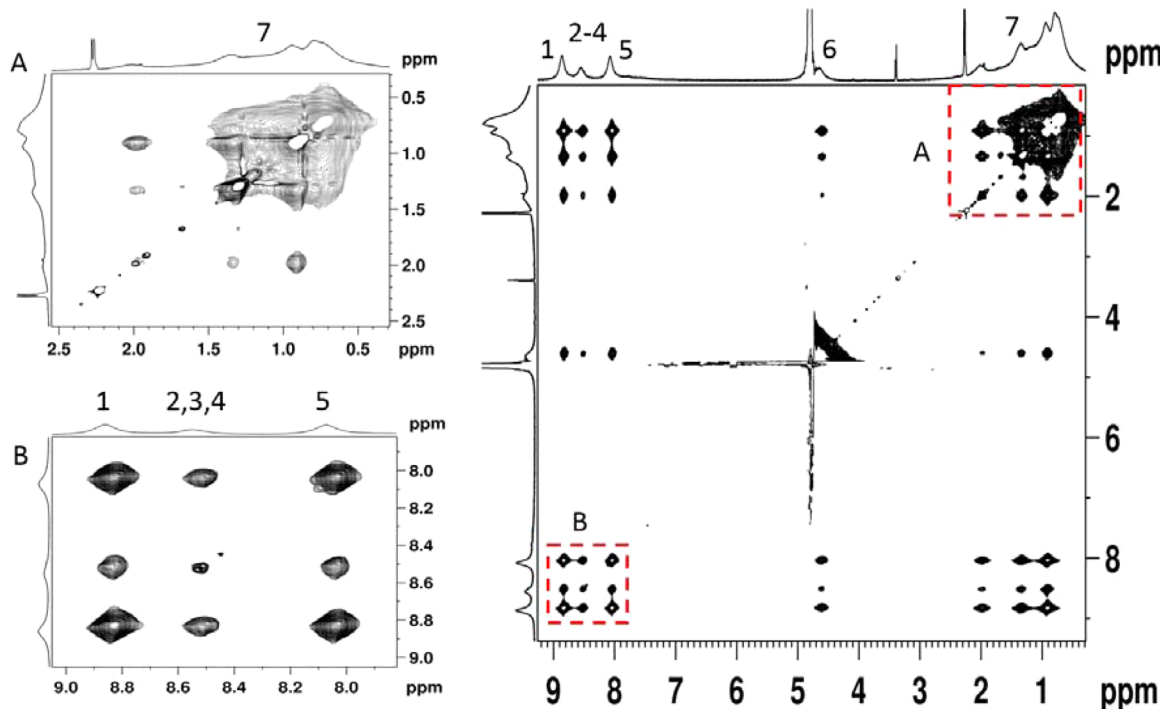
protons of the benzene headgroup of the DBS anion (4H, 5H) indicating that imidazolium cations are present slightly deeper in the palisade layer of vesicles. Other cross-peaks which show strong interactions between (i) alkyl chain (8H) and aromatic proton (1–5H), (ii) the N–CH<sub>2</sub> (7H) and N–CH<sub>3</sub>(6H) group with alkyl chain, and (iii) aromatic protons (1–5H) and alkyl chain protons (8H) collectively suggest that there is a compact and efficient packing between the cation and anion in 100 mM NaBr solution. These cross-peaks are given in the Supporting Information (Figure S4) with expanded form.

Figure 12A (expanded form) also shows cross peak between the alkyl chain of butyl and the dodecyl chain (7H) suggesting that both alkyl chains are parallel. Figure 12B also shows strong interaction between aromatic protons of the pyridinium cation (1–3H) and benzene of the DBS group (4H and 5H) in anion indicating more compact and efficient packing compared to  $[C_4\text{mim}]$ DBS due to the similar symmetry of aromatic rings.

Other cross-peaks generated are given in the Supporting Information (Figure S4) which shows an interaction between aromatic protons (1–5H) and alkyl chain protons (7H), an interaction of the N–CH<sub>2</sub> group of cations (6H) with aromatic protons of anion (4H, 5H), and the alkyl chain of the dodecyl group (6H).

#### 4. CONCLUSION

Dodecylbenzenesulfonate-based anionic surface-active ionic liquids (DBS-ILs) with onium counterions, 1-butyltrimethylammonium ( $N_{1114}$ ), 1-butyl-3-methylimidazolium ( $[C_4\text{mim}]$ ), and 1-butylpyridinium ( $[C_4\text{Py}]$ ), have been found to be better surface active than their conventional analogue  $[Na]$ DBS. The colloidal solutions of DBS-ILs predominantly formed micelles of  $\sim 10$  nm hydrodynamic diameter with a very small number of unilamellar vesicles, whereas colloidal solution of  $[Na]$ DBS contained only micelles and some loose aggregates. Micelle to



**Figure 12.** NOESY spectrum of  $[C_4\text{Py}]$ DBS in deuterated 100 mM NaBr solution. These NOEs originate from (A) interaction between alkyl chain protons of both butyl and dodecyl groups and (B) aromatic proton (DBS) interactions with the pyridinium proton.

vesicle transition (MVT) could be induced in the colloidal solutions of DBS-ILs in the presence of NaBr, whereas no such transition was observed in conventional  $[\text{Na}]$ DBS solutions. DBS-IL solutions containing NaBr formed mostly unilamellar vesicles as evidenced from the cryo-TEM images. 2D NOESY experiments suggested a compact and efficient packing of cations and anions in the vesicles. The studies show that novel anionic surface-active ionic liquid surfactants (SAILS) can be developed by judicious choice of cations and anions having an electron-rich  $\pi$  system for the formation of cation– $\pi$  or  $\pi$ – $\pi$  interaction-driven bilayer structures. This work will advance the utilization of SAILS for different applications such as stimuli-responsive vehicles for drug delivery, *in vivo* transfection activity of genes into cells, and templates for synthesis of nanomaterials.

## ASSOCIATED CONTENT

### Supporting Information

NMR spectra of synthesized DBS-ILs, conductivity plots of  $[\text{Na}]$ DBS and DBS-ILs in aqueous medium at 298.15 K, DLS distributions of  $[\text{Na}]$ DBS and DBS-ILs at 4 mM, 10 mM, 40 mM, 60 mM, and 100 mM in aqueous medium and salt solutions, 2D NOESY spectra of  $[C_4\text{mim}]$ DBS and  $[C_4\text{Py}]$ DBS with expanded forms. Tables S1 and S2 containing refractive index and viscosity data of colloidal solutions of DBS-ILs and  $[\text{Na}]$ DBS in water and in aqueous electrolyte solutions and elemental compositions of synthesized DBS-ILs (Table S3) are provided. This material is available free of charge via the Internet at <http://pubs.acs.org>.

## AUTHOR INFORMATION

### Corresponding Author

\*E-mail: mailme\_arvind@yahoo.com; arvind@csmcri.org. Tel.: +91-278-2567039. Fax: +91-278-2567562.

### Author Contributions

<sup>†</sup>Authors K.S.R. and P.S.G. have contributed equally to this work.

### Notes

The authors declare no competing financial interest.

## ACKNOWLEDGMENTS

We thank the Department of Science and Technology (DST), Government of India, for the financial support for this work (No. SB/S1/PC-104/2012). K. S. Rao is thankful to CSIR for SRF fellowship, and P. S. Gehlot is thankful to UGC for JRF fellowship. Analytical division & central instrumentation facility of CSMCRI is also acknowledged for helping with the sample characterization.

## REFERENCES

- (1) Fendler, J. H. *Membrane Mimetic Chemistry*; Wiley-Interscience: New York, 1982.
- (2) Lasic, D. D. *Liposomes: From Physics to Applications*; Elsevier, Amsterdam, 1993.
- (3) Wang, A. Z.; Langer, R.; Farokhzad, O. C. Nanoparticle Delivery of Cancer Drugs. *Annu. Rev. Med.* **2012**, *63*, 185–198.
- (4) Torchilin, V. P. Recent Advances with Liposomes as Pharmaceutical Carriers. *Nat. Rev. Drug Discovery* **2005**, *4*, 145–160.
- (5) Fathi, M.; Mozafari, M. R.; Mohebbi, M. Nanoencapsulation of Food Ingredients using Lipid based Delivery Systems. *Trends Food Sci. Technol.* **2012**, *23*, 13–27.
- (6) Mozafari, M. R.; Johnson, C.; Hatziantoniou, S.; Demetzos, C. Nanoliposomes and Their Applications in Food Nanotechnology. *J. Liposome Res.* **2008**, *18*, 309–327.
- (7) Betz, G.; Aepli, A.; Menshutina, N.; Leuenberger, H. In Vivo Comparison of Various Liposome Formulations for Cosmetic Application. *Int. J. Pharm.* **2005**, *296*, 44–54.
- (8) Barani, H.; Montazer, M. A Review on Applications of Liposomes in Textile Processing. *J. Liposome Res.* **2008**, *18*, 249–262.

- (9) Yang, P.; Lipowsky, R.; Dimova, R. Nanoparticle Formation in Giant Vesicles: Synthesis in Biomimetic Compartments. *Small* **2009**, *5*, 2033–2037.
- (10) Jiang, Z.; Liu, J.; Sun, K.; Dong, J.; Li, X.; Mao, S.; Du, Y.; Liu, M. pH- and Concentration-Induced Micelle-to-Vesicle Transitions in Pyrrolidone-based Gemini Surfactants. *Colloid Polym. Sci.* **2014**, *292*, 739–747.
- (11) González, Y. I.; Nakanishi, H.; Stjerndahl, M.; Kaler, E. W. Influence of pH on the Micelle-to-Vesicle Transition in Aqueous Mixtures of Sodium Dodecyl Benzenesulfonate with Histidine. *J. Phys. Chem. B* **2005**, *109*, 11675–11682.
- (12) Uda, R. M.; Tanabe, T.; Nakahara, Y.; Kimura, K. Photoinduced Micelle-to-Vesicle Transition and Encapsulation of Glucose by Photoresponsive Malachite Green Leuconitrile derivative. *Soft Matter* **2008**, *4*, 560–563.
- (13) Yin, H.; Zhou, Z.; Huang, J.; Zheng, R.; Zhang, Y. Temperature-Induced Micelle to Vesicle Transition in the Sodium Dodecylsulfate/Dodecytriethylammonium Bromide System. *Angew. Chem., Int. Ed. 2003*, *42*, 2188–2191.
- (14) Oda, R.; Bourdieu, L. Micelle to Vesicle Transition Induced by Cosurfactant: Rheological Study and Direct Observations. *J. Phys. Chem. B* **1997**, *101*, 5913–5916.
- (15) Zhai, L.; Zhao, M.; Sun, D.; Hao, J.; Zhang, L. Salt-Induced Vesicle Formation from Single Anionic Surfactant SDBS and Its Mixture with LSB in Aqueous Solution. *J. Phys. Chem. B* **2005**, *109*, 5627–5630.
- (16) Mohanty, A.; Patra, T.; Dey, J. Salt-Induced Vesicle to Micelle Transition in Aqueous Solution of Sodium N-(4-n-Octyloxybenzoyl)-L-valinate. *J. Phys. Chem. B* **2007**, *111*, 7155–7159.
- (17) Söderman, O.; Herrington, K. L.; Kaler, E. W.; Miller, D. D. Transition from Micelles to Vesicles in Aqueous Mixtures of Anionic and Cationic Surfactants. *Langmuir* **1997**, *13*, 5531–5538.
- (18) Li, W.; Yang, Y.; Luo, T.; Zhang, J.; Han, B. CO<sub>2</sub>-induced Micelle to Vesicle Transition in Zwitterionic-Anionic Surfactant Systems. *Phys. Chem. Chem. Phys.* **2014**, *16*, 3640–3647.
- (19) Li, W.; Zhang, J.; Zhao, Y.; Hou, M.; Han, B.; Yu, C.; Ye, J. Reversible Switching of a Micelle-to-Vesicle Transition by Compressed CO<sub>2</sub>. *Chem.—Eur. J.* **2010**, *16*, 1296–1305.
- (20) Baker, G. A.; Pandey, S.; Pandey, S.; Baker, S. N. A New Class of Cationic Surfactants inspired by N-alkyl-N-methyl Pyrrolidinium Ionic Liquids. *Analyst* **2004**, *129*, 890–892.
- (21) Singh, T.; Kumar, A. Aggregation Behavior of Ionic Liquids in Aqueous Solutions: Effect of Alkyl Chain Length, Cations, and Anions. *J. Phys. Chem. B* **2007**, *111*, 7843–7851.
- (22) Baltazar, Q. Q.; Chandawalla, J.; Sawyer, K.; Anderson, J. L. Interfacial and Micellar Properties of Imidazolium-based Monocationic and Dicationic Ionic Liquids. *Colloids Surf. A* **2007**, *302*, 150–156.
- (23) Ao, M.; Xu, G.; Zhu, Y.; Bai, Y. Synthesis and Properties of Ionic Liquid-type Gemini Imidazolium Surfactants. *J. Colloid Interface Sci.* **2008**, *326*, 490–495.
- (24) Bhadani, A.; Singh, S. Synthesis and Properties of Thioether Spacer Containing Gemini Imidazolium Surfactants. *Langmuir* **2011**, *27*, 14033–14044.
- (25) Miskolczy, Z.; Sebők-Nagy, K.; Biczók, L.; Göktürk, S. Aggregation and Micelle Formation of Ionic Liquids in Aqueous Solution. *Chem. Phys. Lett.* **2004**, *400*, 296–300.
- (26) Jiao, J.; Dong, B.; Zhang, H.; Zhao, Y.; Wang, X.; Wang, R.; Yu, L. Aggregation Behaviors of Dodecyl Sulfate-Based Anionic Surface Active Ionic Liquids in Water. *J. Phys. Chem. B* **2012**, *116*, 958–965.
- (27) Trivedi, T. J.; Rao, K. S.; Singh, T.; Mandal, S. K.; Sutradhar, N.; Panda, A. B.; Kumar, A. Task-specific, Biodegradable Amino Acid Ionic Liquid Surfactants. *ChemSusChem* **2011**, *4*, 604–608.
- (28) Rao, K. S.; Singh, T.; Trivedi, T. J.; Kumar, A. Aggregation Behavior of Amino Acid Ionic Liquid Surfactants in Aqueous Media. *J. Phys. Chem. B* **2011**, *115*, 13847–13853.
- (29) Brown, P.; Butts, C.; Dyer, R.; Eastoe, J.; Grillo, I.; Guittard, F.; Rogers, S.; Heenan, R. Anionic Surfactants and Surfactant Ionic Liquids with Quaternary Ammonium Counterions. *Langmuir* **2011**, *27*, 4563–4571.
- (30) Brown, P.; Butts, C. P.; Eastoe, J.; Fermin, D.; Grillo, I.; Lee, H.; Parker, D.; Plana, D.; Richardson, R. M. Anionic Surfactant Ionic Liquids with 1-Butyl-3-methyl-imidazolium Cations: Characterization and Application. *Langmuir* **2012**, *28*, 2502–2509.
- (31) Alvarez, V. H.; Mattedi, S.; Martin-Pastor, M.; Aznar, M.; Iglesias, M. Synthesis and Thermophysical Properties of two New Protic Long-Chain Ionic Liquids with the Oleate anion. *Fluid Phase Equilib.* **2010**, *299*, 42–50.
- (32) Rao, K. S.; Gehlot, P. S.; Trivedi, T. J.; Kumar, A. Self-assembly of New Surface Active Ionic Liquids based on Aerosol-OT in Aqueous media. *J. Colloid Interface Sci.* **2014**, *428*, 267–275.
- (33) Villa, C. C.; Moyano, F.; Ceolin, M.; Silber, J. J.; Falcone, R. D.; Correa, N. M. A Unique Ionic Liquid with Amphiphilic Properties That Can Form Reverse Micelles and Spontaneous Unilamellar Vesicles. *Chem.—Eur. J.* **2012**, *18*, 15598–15601.
- (34) Brown, P.; Butts, C. P.; Eastoe, J.; Grillo, I.; James, C.; Khan, A. New Catanionic Surfactants with Ionic Liquid Properties. *J. Colloid Interface Sci.* **2013**, *395*, 185–189.
- (35) Rao, K. S.; Trivedi, T. J.; Kumar, A. Aqueous-Biamphiphilic Ionic Liquid Systems: Self-Assembly and Synthesis of Gold Nano-crystals/Microplates. *J. Phys. Chem. B* **2012**, *116*, 14363–14374.
- (36) Tondo, D. W.; Leopoldino, E. C.; Souza, B. S.; Micke, G. A.; Costa, A. C. O.; Fiedler, H. D.; Bunton, C. A.; Nome, F. Synthesis of a New Zwitterionic Surfactant Containing an Imidazolium Ring. Evaluating the Chameleon-Like Behavior of Zwitterionic Micelles. *Langmuir* **2010**, *26*, 15754–15760.
- (37) Liu, X.; Dong, L.; Fang, Y. A Novel Zwitterionic Imidazolium-Based Ionic Liquid Surfactant: 1-Carboxymethyl-3-Dodecylimidazolium Inner Salt. *J. Surfactants Deterg.* **2011**, *14*, 497–504.
- (38) Wang, X.; Liu, J.; Yu, L.; Jiao, J.; Wang, R.; Sun, L. Surface Adsorption and Micelle formation of Imidazolium-Based Zwitterionic Surface Active Ionic Liquids in Aqueous Solution. *J. Colloid Interface Sci.* **2013**, *391*, 103–110.
- (39) Rao, V. G.; Ghosh, S.; Ghatak, C.; Mandal, S.; Brahmachari, U.; Sarkar, N. Phase boundaries, Structural characteristics, and NMR Spectra of Ionic liquid-in-oil Microemulsions containing Double Chain Surface Active Ionic Liquid: A Comparative Study. *J. Phys. Chem. B* **2012**, *116*, 2850–2855.
- (40) Cornellas, A.; Perez, L.; Comelles, F.; Ribosa, I.; Manresa, A.; Teresa Garcia, M. Self-aggregation and Antimicrobial Activity of Imidazolium and Pyridinium-Based Ionic Liquids in Aqueous Solution. *J. Colloid Interface Sci.* **2011**, *355*, 164–171.
- (41) Garcia, T. M.; Ribosa, I.; Perez, L.; Manresa, A.; Comelles, F. Aggregation Behavior and Antimicrobial Activity of Ester-Functionalized Imidazolium- and Pyridinium-Based Ionic Liquids in Aqueous Solution. *Langmuir* **2013**, *29*, 2536–2545.
- (42) Garcia, M. T.; Ribosa, I.; Perez, L.; Manresa, A.; Comelles, F. Self-assembly and Antimicrobial Activity of Long-Chain Amide-Functionalized Ionic Liquids in Aqueous Solution. *Colloids Surf. B* **2014**, *123*, 318–325.
- (43) Souza, B. S.; Leopoldino, E. C.; Tondo, D. W.; Dupont, J.; Nome, F. Imidazolium-Based Zwitterionic Surfactant: A New AmphiphilicPd Nanoparticle Stabilizing Agent. *Langmuir* **2012**, *28*, 833–840.
- (44) Gao, Y.; Voigt, A.; Zhou, M.; Sundmacher, K. Synthesis of Single-Crystal Gold Nano- and Microprisms Using a Solvent-Reductant-Template Ionic Liquid. *Eur. J. Inorg. Chem.* **2008**, *24*, 3769–3775.
- (45) Rao, K. S.; Singh, T.; Kumar, A. Aqueous-Mixed Ionic Liquid System: Phase Transitions and Synthesis of Gold Nanocrystals. *Langmuir* **2011**, *27*, 9261–9269.
- (46) Li, N.; Zhang, S.; Zheng, L.; Dong, B.; Li, X.; Yu, L. Aggregation Behavior of Long-Chain Ionic Liquids in an Ionic Liquid. *Phys. Chem. Chem. Phys.* **2008**, *10*, 4375–4377.
- (47) Shi, L.; Li, N.; Zheng, L. Aggregation Behavior of Long-Chain N-Aryl Imidazolium Bromide in a Room Temperature Ionic Liquid. *J. Phys. Chem. C* **2011**, *115*, 18295–18301.
- (48) Shi, L.; Zheng, L. Aggregation Behavior of Surface Active Imidazolium Ionic Liquids in Ethylammonium Nitrate: Effect of Alkyl

Chain Length, Cations, and Counterions. *J. Phys. Chem. B* **2012**, *116*, 2162–2172.

(49) Rao, K. S.; So, S.; Kumar, A. Vesicles and Reverse Vesicles of an Ionic Liquid in Ionic Liquids. *Chem. Commun.* **2013**, *49*, 8111–8113.

(50) Smirnova, N. A.; Vanin, A. A.; Safonova, E. A.; Pukinsky, I. B.; Anufriev, Y. A.; Makarov, A. L. Self-Assembly in Aqueous Solutions of ImidazoliumIonic Liquids and their Mixtures with an Anionic Surfactant. *J. Colloid Interface Sci.* **2009**, *336*, 793–802.

(51) Yuan, J.; Bai, X.; Zhao, M.; Zheng, L. C<sub>12</sub>mimBr Ionic Liquid/SDS Vesicle Formation and Use as Template for the Synthesis of Hollow Silica Spheres. *Langmuir* **2010**, *26*, 11726–11731.

(52) Singh, K.; Marangoni, D. G.; Quinn, J. G.; Singer, R. D. Spontaneous Vesicle Formation with an Ionic Liquid Amphiphile. *J. Colloid Interface Sci.* **2009**, *335*, 105–111.

(53) Ghosh, S.; Ghatak, C.; Banerjee, C.; Mandal, S.; Kuchlyan, J.; Sarkar, N. Spontaneous Transition of Micelle–Vesicle–Micelle in a Mixture of Cationic Surfactant and Anionic Surfactant-like Ionic Liquid: A Pure Non-lipid Small Unilamellar Vesicular Template Used for Solvent and Rotational Relaxation Study. *Langmuir* **2013**, *29*, 10066–10076.

(54) Mandal, S.; Kuchlyan, J.; Banik, D.; Ghosh, S.; Banerjee, C.; Khorwal, V.; Sarkar, N. Ultrafast FRET to Study Spontaneous Micelle-to-Vesicle Transitions in an Aqueous Mixed Surface-Active Ionic-Liquid System. *ChemPhysChem* **2014**, *15*, 3544–3553.

(55) Wang, H.; Zhang, L.; Wang, J.; Li, Z.; Zhang, S. The First Evidence for Unilamellar Vesicle Formation of Ionic Liquids in Aqueous Solutions. *Chem. Commun.* **2013**, *49*, 5222–5224.

(56) Gu, Y.; Shi, L.; Cheng, X.; Lu, F.; Zheng, L. Aggregation Behavior of 1-Dodecyl-3-methylimidazolium Bromide in Aqueous Solution: Effect of Ionic Liquids with Aromatic Anions. *Langmuir* **2013**, *29*, 6213–6220.

(57) Anouti, M.; Sizaret, P.; Ghimbeu, C.; Galiano, H.; Lemordant, D. Physicochemical Characterization of Vesicles Systems Formed in Mixtures of Protic Ionic Liquids and Water. *Colloids Surf., A* **2012**, *395*, 190–198.

(58) Nguyen, K. T.; Nguyen, A. V. In Situ Investigation of Halide Co-ion Effects on SDS Adsorption at Air–Water Interfaces. *Soft Matter* **2014**, *10*, 6556–6563.

(59) Rosen, M. J. *Surfactants and Interfacial Phenomena*, 2nd ed.; Wiley: New York, 1989.

(60) Eastoe, J.; Nave, S.; Downer, A.; Paul, A.; Rankin, A.; Tribe, K.; Penfold, J. Adsorption of Ionic Surfactants at the Air-Solution Interface. *Langmuir* **2000**, *16*, 4511–4518.

(61) Villeneuve, M.; Ootsu, R.; Ishiwata, M.; Nakahara, H. Research on the Vesicle-Micelle Transition by <sup>1</sup>H NMR Relaxation Measurement. *J. Phys. Chem. B* **2006**, *110*, 17830–17839.

(62) Meyer, E. A.; Castellano, R. K.; Diederich, F. Interactions with Aromatic Rings in Chemical and Biological Recognition. *Angew. Chem., Int. Ed.* **2003**, *42*, 1211–1239.

(63) Gallivan, J. P.; Dougherty, D. A. A Computational Study of Cation-π Interactions vs Salt Bridges in Aqueous Media: Implications for Protein Engineering. *J. Am. Chem. Soc.* **2000**, *122*, 870–874.

(64) Lu, Q.; Oh, D. X.; Lee, Y.; Jho, Y.; Hwang, D. S.; Zeng, H. Nanomechanics of Cation-p Interactions in Aqueous Solution. *Angew. Chem., Int. Ed.* **2013**, *52*, 3944–3948.

(65) Amunugama, R.; Rodgers, M. T. The Influence of Substituents on Cation-π Interactions. 4. Absolute Binding Energies of Alkali Metal Cation–Phenol Complexes Determined by Threshold Collision-Induced Dissociation and Theoretical Studies. *J. Phys. Chem. A* **2002**, *106*, 9718–9728.